THE JOURNAL OF PHYSICAL CHEMISTRY C

Article

pubs.acs.org/JPCC

Comparison of the Photoelectrochemical Behavior of H-Terminated and Methyl-Terminated Si(111) Surfaces in Contact with a Series of One-Electron, Outer-Sphere Redox Couples in CH_3CN

Ronald L. Grimm, Matthew J. Bierman, Leslie E. O'Leary, Nicholas C. Strandwitz, Bruce S. Brunschwig, and Nathan S. Lewis*

Beckman Institute and Kavli Nanoscience Institute, Division of Chemistry and Chemical Engineering, 127-72, 210 Noyes Laboratory, California Institute of Technology, Pasadena, California 91125, United States

Supporting Information

ABSTRACT: The photoelectrochemical behavior of methyl-terminated p-type and n-type Si(111) surfaces was determined in contact with a series of one-electron, outer-sphere, redox couples that span >1 V in the Nernstian redox potential, $E(A/A^-)$, of the solution. The dependence of the current vs potential data, as well as of the open-circuit photovoltage, V_{oc}, on $E(A/A^-)$ was compared to the behavior of H-terminated p-type and n-type Si(111) surfaces in contact with these same electrolytes. For a particular $E(A/A^-)$ value, CH_3-terminated p-Si(111) electrodes showed lower V_{oc} values than H-terminated p-Si(111) electrodes, whereas CH_3-terminated n-Si(111) electrodes showed higher V_{oc} values than H-terminated n-Si(111) electrodes. Under 100 mW cm^{-2} of ELH-simulated Air Mass 1.5 illumination, n-type H−Si(111) and CH_3−Si(111) electrodes both demonstrated nonrectifying behavior with no photovoltage at very negative values of $E(A/A^-)$ and produced limiting V_{oc} values of >0.5 V at very positive values of $E(A/A^-)$. Illuminated p-type H−Si(111) and CH_3−Si(111) electrodes produced no photovoltage at positive values of $E(A/A^-)$ and produced limiting V_{oc} values in excess of 0.5 V at very negative values of $E(A/A^-)$. In contact with CH_3CN-octamethylferrocene$^{+/0}$, differential capacitance vs potential experiments yielded a −0.40 V shift in flat-band potential for CH_3-terminated n-Si(111) surfaces relative to H-terminated n-Si(111) surfaces. Similarly, in contact with CH_3CN-1,1′-dicarbomethoxycobaltocene$^{+/0}$, the differential capacitance vs potential data indicated a −0.25 V shift in the flat-band potential for CH_3-terminated p-Si(111) electrodes relative to H-terminated p-Si(111) electrodes. The observed trends in V_{oc} vs $E(A/A^-)$, and the trends in the differential capacitance vs potential data are consistent with a negative shift in the interfacial dipole as a result of methylation of the Si(111) surface. The negative dipole shift is consistent with a body of theoretical and experimental comparisons of the behavior of CH_3−Si(111) surfaces vs H−Si(111) surfaces, including density functional theory of the sign and magnitude of the surface dipole, photoemission spectroscopy in ultrahigh vacuum, the electrical behavior of Hg/Si contacts, and the pH dependence of the current−potential behavior of Si electrodes in contact with aqueous electrolytes.

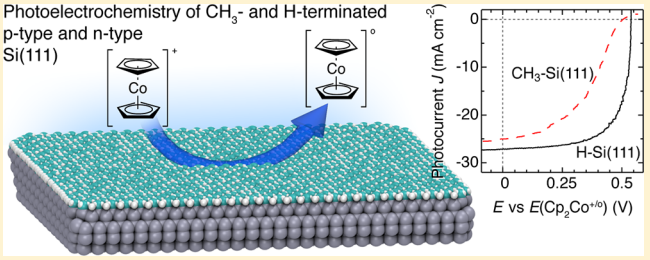

I. INTRODUCTION

To use semiconductor/liquid contacts for photoelectrochemical water splitting, the band-edge potentials must be favorably positioned relative to the formal potentials of the fuel-forming reactions, to ensure that the half-reactions for H_2 evolution and O_2 evolution are allowed thermodynamically under standard conditions.[1,2] Many semiconductors, such as TiO_2 and WO_3, can produce the required photovoltage, but one (or both) of the band-edge positions of such materials are not properly positioned to thermodynamically effect water splitting in the absence of an externally applied bias voltage.[1] Hence, methods to manipulate, and to control chemically, the band-edge positions at semiconductor/liquid interfaces are of interest.

Silicon is one semiconductor of interest, primarily for use as a photocathode.[3] Cathodic protection of Si would minimize the oxidatively driven formation of electrically insulating SiO_x overlayers.[3] Si(111) surfaces provide nearly ideal systems for the exploration of band-edge manipulation derived from chemical functionalization methods, due to the well-defined chemical and structural properties of the H-terminated Si(111) surface.[4] Additionally, Si(111) surfaces can be functionalized with methyl groups through the use of a two-step chlorination/alkylation process to produce well-ordered, chemically well-defined, CH_3−Si(111) surfaces.[4−11] Such surfaces have essentially complete coverage of Si−C bonds on an unreconstructed Si(111) surface. CH_3−Si(111) surfaces have been characterized by X-ray photoelectron spectroscopy,[8,9,12,13] scanning tunneling spectroscopy,[10] infrared vibrational spec-

Received: September 11, 2012
Revised: October 12, 2012
Published: October 13, 2012

Table 1. Summary of Experimental Conditions and Results[a]

	potentials vs $E^{o\prime}(Fc^{+/0})$ (V)		concentrations (mM)		effective potentials vs SCE (V)		V_{oc} under 100 mW cm^{-2} illumination (V)			
	$E(A/A^-)$	$E^{o\prime}(A/A^-)$	ox	red	$E_{eff}(A/A^-)$ for p-Si	$E_{eff}(A/A^-)$ for n-Si	p-type H–Si(111)	p-type CH_3–Si(111)	n-type H–Si(111)	n-type CH_3–Si(111)
dimethylcobaltocene$^{+/0}$ $Me_2Cp_2Co^{+/0}$	−1.340	−1.410	54.9	*	−0.987	−1.003	0.578(21)	0.556(31)		
cobaltocene$^{+/0}$ $Cp_2Co^{+/0}$	−1.222	−1.331	54.6	1.2	−0.867	−0.857	0.538(40)	0.508(38)	0.005(7)	0.001(1)
octamethylnickelocene$^{+/0}$ $Me_8Cp_2Ni^{+/0}$	−1.016	−0.990	7.4	18.3	−0.713	−0.720	0.501(30)	0.410(28)		0.030(10)
methyl viologen$^{2+/+\bullet}$ $MV^{2+/+\bullet}$	−0.830	−0.890	1.5	*	−0.570	−0.408	0.530(51)	0.310(31)	0.007(4)	0.102(17)
1,1′-dicarbomethoxycyclopentadienylcobaltocene$^{+/0}$ $(CpCO_2CH_3)_2Co^{+/0}$	−0.672	−0.763	37.7	1.8	−0.327	−0.317	0.447(48)	0.166(19)	0.015(11)	0.180(10)
nickelocene$^{+/0}$ $Cp_2Ni^{+/0}$	−0.490	−0.445	*	65.0	−0.182	−0.222	0.261(54)	0.040(17)	0.120(20)	0.320(24)
decamethylferrocene$^{+/0}$ $Cp^*_2Fe^{+/0}$	−0.418	−0.468	12.1	0.8	−0.124	−0.042	0.294(25)	0.005(10)	0.111(11)	0.419(11)
octamethylferrocene$^{+/0}$ $Me_8Cp_2Fe^{+/0}$	−0.353	−0.406	23.5	2.7	−0.020	−0.008	0.217(18)	0.010(8)	0.173(14)	0.452(30)
dimethylferrocene$^{+/0}$ $Me_2Cp_2Fe^{+/0}$	−0.182	−0.100	1.7	51.4	0.084	0.087	0.025(15)		0.341(25)	0.511(25)
ferrocene$^{+/0}$ $Cp_2Fe^{+/0}$, or $Fc^{+/0}$	−0.065	0	4.5	54.0	0.226	0.203	0.015(13)		0.450(20)	0.520(29)
acetylferrocene$^{+/0}$ $(CpCOCH_3)CpFe^{+/0}$	0.153	0.261	*	54.9	0.408	0.420			0.531(19)	0.539(30)

[a]The Nernstian redox cell potentials, $E(A/A^-)$, and formal potentials, $E^{o\prime}(A/A^-)$, for each redox couple employed are reported vs the ferrocene formal potential $E^{o\prime}(\text{ferrocene}^{+/0})$, $E^{o\prime}(Fc^{+/0})$, in CH_3CN–1.0 M $LiClO_4$. The solution concentrations are reported in mM except for solutions in which one of the species was generated in situ via bulk electrolysis, which are denoted by an asterisk (*). Effective solution potentials, $E_{eff}(A/A^-)$, are listed to facilitate intercomparison of the open-circuit photovoltage, V_{oc}, values and are calculated based on $E(A/A^-)$ and the concentrations of redox species. The $E_{eff}(A/A^-)$ values are tabulated relative to the potential of the saturated calomel electrode, SCE, as adjusted by the experimentally determined conversion, $E^{o\prime}(Fc^{+/0}) = +0.311$ V vs SCE for ferrocene$^{+/0}$ in CH_3CN–1.0 M $LiClO_4$. All of the V_{oc} values represent the average open-circuit photovoltage for multiple electrodes under 100 mA cm^{-2} of ELH-type tungsten-halogen illumination, with standard deviations in parentheses.

dx.doi.org/10.1021/jp308461q | J. Phys. Chem. C 2012, 116, 23569–23576

troscopy,[6,8] low-energy electron diffraction,[13] temperature programmed desorption,[8] and high-resolution electron-energy loss spectroscopy,[14] among other techniques.[6]

In contact with ultrahigh vacuum (UHV), a combination of synchrotron-based soft X-ray photoelectron spectroscopy and ultraviolet photoelectron spectroscopy measurements indicated that the CH_3−Si(111) surface had an interfacial dipole of −0.37 eV,[9] as compared to an interfacial dipole of +0.12 eV for the H-terminated Si(111) surface.[15−17] Current density vs potential (J−E) and differential capacitance vs potential (C_{diff}^{-2}−E) measurements with n-type Si indicated an increase in barrier height of ∼0.55 eV for Hg/CH_3−Si(111) junctions relative to Hg/H−Si(111) contacts at 300 K. Consistently, the barrier height for p-type Si surfaces decreased by >0.67 eV for CH_3−Si(111)/Hg contacts at 300 K relative to Hg/H−Si(111) contacts at 85 K. The direction and magnitude of the dipole on CH_3−Si(111) surfaces has also been investigated theoretically and is consistent with expectations based on the electronegativities of the Si, C and H species involved in the surface bonding.[18]

We report herein the magnitude and direction of band-edge shifts for various CH_3−Si(111)/CH_3CN contacts, relative to the energetics of analogous H−Si(111)/CH_3CN interfaces. Both J−E data and C_{diff}^{-2}−E data were collected for a series of one-electron, outer-sphere, redox species that span a >1 V range in electrochemical potential, to compare systematically the photoelectrochemical behavior of n-type and p-type CH_3−Si(111) electrodes to that of n-type and p-type H−Si(111) electrodes.

II. EXPERIMENTAL SECTION

A. Chemicals and Silicon Wafers. Electrochemistry was performed in CH_3CN (99.8% anhydrous, Sigma-Aldrich) that contained lithium perchlorate ($LiClO_4$, 99.99% battery grade, Sigma Aldrich) as the supporting electrolyte. The CH_3CN was dried by use of a column of activated Al_2O_3. All 18 MΩ cm resistivity water was obtained from a Barnstead Nanopure system.

Prior to use, boron-doped, 0.24 Ω cm resistivity, p-type Si(111) (Addison Engineering, San Jose, California, with an acceptor density, N_A = 7.7 × 10^{16} cm^{-3}), and phosphorus-doped, 1.5 Ω cm resistivity, n-type Si(111) (Silicon Inc., Boise, Idaho, with a donor density, N_D = 3.2 × 10^{15} cm^{-3}) samples, both polished on one side and 381 ± 25 μm thick, were diced into ∼2 × 1 cm pieces. The Si was sonicated and subsequently was rinsed in acetone (OmniSolv, EMD) followed by a rinse with isopropyl alcohol (ACS grade, EMD). The Si surfaces were then cleaned using an RCA SC-1 procedure followed by an SC-2 etch.[19] Samples were etched for 10 s in a 6 M HF (aq) solution prepared by dilution of 49 wt % HF (aq) (semiconductor grade, Transene Company Inc., Danvers, Massachusetts) in H_2O. The Si samples were rinsed with copious amounts of H_2O and were dried in a stream of Ar (g). Silicon samples that were to be converted into CH_3−Si(111) electrodes were etched further for 15 min in degassed 11 M (48 wt %) NH_4F (aq) (Transene Company Inc.) and then were transferred immediately to a flush box for surface methylation.

B. Surface Functionalization and Characterization. Both p-type H−Si(111) and n-type H−Si(111) surfaces were methylated using a two-step chlorination/alkylation procedure.[7] In a N_2 (g)-purged flush box, H−Si(111) samples were chlorinated at 90 ± 2 °C for 45 min in a saturated solution of PCl_5 (purum, ≥ 98.0%, Sigma-Aldrich) in chlorobenzene (anhydrous, 99.8%, Sigma Aldrich). Following a rinse with chlorobenzene and a subsequent rinse with tetrahydrofuran (THF, anhydrous, ≥ 99.9%, inhibitor-free, Sigma Aldrich), the Cl−Si(111) surfaces were exposed to methylmagnesium chloride (3 M in THF, Sigma Aldrich, diluted to 1 M with THF) for 3−4 h at 60 ± 2 °C. The resulting CH_3−Si(111) surfaces were rinsed with THF, followed by a rinse in CH_3OH (anhydrous, 99.8%, Sigma Aldrich). The samples were removed from the flush box and were rinsed further in CH_3OH, sonicated in CH_3CN, and then rinsed with H_2O. Functionalized CH_3−Si(111) samples were diced, and electrodes were prepared immediately. Following an 8 day exposure to ambient air in the dark, X-ray photoelectron spectroscopy (XPS) verified the lack of significant of oxide formation on the CH_3−Si(111) samples (see the Supporting Information).

C. Electrode Fabrication. Ohmic contacts to the back side of the p-Si(111) electrodes that were used for differential capacitance−potential experiments were formed by evaporation of 300 nm of Al (Denton Vacuum, Moorestown, New Jersey), followed by a 30 min anneal at 450 °C under 5 vol % H_2 (g)/95% N_2 (g). The aluminum contact was formed prior to the chlorination/alkylation procedure, and care was taken to physically isolate the aluminum-coated side of the wafer from the side that was exposed to the chlorination and to the alkylation solutions. For both n-type and p-type electrodes that were used in the J−E studies, ohmic contacts were formed by using a diamond tipped scribe to scratch a Ga−In eutectic alloy into pieces of the Si wafer. The ohmically contacted Si samples were affixed to a tinned Cu wire by use of high purity, conductive, Ag paint (SPI Supplies, West Chester, Pennsylvania). The Cu wire was then threaded through a Pyrex tube until only the wafer face was exposed perpendicular to the tube length. The electrode was then sealed with Loctite 9460 epoxy. The exposed areas of Si(111) were 1−3 mm^2 for electrodes used in J−E studies and were 0.7−0.9 cm^2 for electrodes used in the differential capacitance−potential studies.

Prior to each photoelectrochemical experiment, H−Si(111) electrode surfaces were etched for 10 s in 6 M HF, rinsed in H_2O, dried in Ar, and immediately transferred to an Ar-purged glovebox. The CH_3−Si(111) electrode surfaces were rinsed sequentially in water, methanol, isopropyl alcohol, and trichloroethylene (spectrophotometric grade, Sigma-Aldrich), dried in Ar, and transferred to the glovebox for photoelectrochemical measurements.

D. Chemicals for Photoelectrochemistry. A series of redox couples having a range of formal potentials, $E^{o\prime}(A/A^-)$, was used in the electrochemical studies (Table 1). For the cobalt-containing compounds, 1,1′-dimethylcobaltocenium ($Me_2Cp_2Co^+PF_6^-$, bis(methylcyclopentadienyl)cobaltocenium hexafluorophosphate) was synthesized from methylcyclopentadienyl lithium, cobalt(II) chloride hydrate, and potassium hexafluorophosphate.[20] 1,1′-Dimethylcobaltocene (Me_2Cp_2Co, bis(methylcyclopentadienyl)cobaltocene) was generated in situ via bulk electrolysis. Cobaltocene (Cp_2Co, bis(cyclopentadienyl)cobalt(II), 98%, Strem) was purified by vacuum sublimation, whereas cobaltocenium ($Cp_2Co^+PF_6^-$, bis(cyclopentadienyl)cobaltocenium hexafluorophosphate, 98%, Sigma-Aldrich) was recrystallized from an ethanol (ACS grade, EMD)/acetonitrile (ACS grade, EMD) mixture and was dried under vacuum. Both 1,1′-dicarbomethoxycobaltocene ($(CpCO_2CH_3)_2Co$, 1,1′-bis(η^5-methoxycarbonylcyclopentadienyl)cobalt) and the oxidized $(CpCO_2CH_3)_2Co^+$

dx.doi.org/10.1021/jp308461q | J. Phys. Chem. C 2012, 116, 23569−23576

species, were synthesized by reacting $CoCl_2$ with the lithium reagent of the functionalized cyclopentadienyl moiety.[21,22]

For the nickel-containing compounds, octamethylnickelocene (Me_8Cp_2Ni, bis(tetramethylcyclopentadienyl)nickel, 98%, Strem) and nickelocene (Cp_2Ni, bis(cyclopentadienyl)nickel, 99%, Strem) were purified by sublimation. Nickelocenium, Cp_2Ni^+, was generated in situ via the electrolysis of Cp_2Ni. Octamethylnickelocenium ($Me_8Cp_2Ni^+BF_4^-$, bis(tetramethylcyclopentadienyl)nickelocenium tetrafluoroborate) was synthesized by the chemical oxidation of octamethylnickelocene, and was purified by recrystallization.[23]

The iron complexes, decamethylferrocene (Cp^*_2Fe, bis(pentamethylcyclopentadienyl)iron, 99%, Strem), octamethylferrocene (Me_8Cp_2Fe, bis(tetramethylcyclopentadienyl)iron, 98%, Strem), 1,1′-dimethylferrocene (Me_2Cp_2Fe, bis(methylcyclopentadienyl)iron, 95%, Sigma-Aldrich), ferrocene (Cp_2Fe, bis(cyclopentadienyl)iron, 99%, Strem), and acetylferrocene ($CpCOCH_3(Cp)Fe$, (acetylcyclopentadienyl)-cyclopentadienyliron, 99.5%, Strem) were purified by sublimation. The salts decamethylferrocenium ($Cp^*_2Fe^+BF_4^-$, bis(pentamethylcyclopentadienyl)ferrocenium tetrafluoroborate), octamethylferrocenium ($Me_8Cp_2Fe^+BF_4^-$, bis(tetramethylcyclopentadienyl)ferrocenium tetrafluoroborate), and 1,1′-dimethylferrocenium ($Me_2Cp_2Fe^+BF_4^-$, bis(methylcyclopentadienyl)ferrocenium tetrafluoroborate) were synthesized by chemical oxidation of the neutral metallocenes.[23] Ferrocenium tetrafluoroborate ($Cp_2Fe^+BF_4^-$, bis(cyclopentadienyl)iron(III) tetrafluoroborate, technical grade, Sigma-Aldrich) was purified by recrystallization. Acetylferrocenium was generated in situ via bulk electrolysis of acetyleferrocene.

Methyl viologen (MV^{2+}, 1,1′-dimethyl-4,4′-bipyridinium dichloride hydrate, 98%, Sigma-Aldrich) was recrystallized from ethanol. The reduced form, $MV^{+\bullet}$, was generated by controlled potential electrolysis of MV^{2+}.

E. Photoelectrochemical Methods. *1. Electrochemical Cells.* Current density vs potential ($J-E$) and area-corrected differential capacitance vs potential ($A^2C_{diff}^{-2}-E$) data were collected in a four-port, cylindrical, flat-bottomed, borosilicate cell that contained 1.0 M $LiClO_4$ in 30 mL of dry CH_3CN. All experiments were performed in an Ar (g)-filled drybox that contained <0.5 ppm of O_2 (g). The reference electrode was a freshly prepared Ag^+/Ag electrode,[29] that was constructed from borosilicate tubing with a Vycor 7930 porous glass frit (Advanced Glass and Ceramics, Holden, Massachusetts) that was attached to the borosilicate by Teflon heat−shrink tubing. Silver wire (0.5 mm diameter, ≥99.99%, Sigma-Aldrich) was abraded with grade 0000 steel wool, etched in 0.10 M HNO_3 (aq) for 10 s, copiously rinsed with water, and transferred to the Ar(g) drybox. The filling solution consisted of ∼1.3 mL of the 1.0 M $LiClO_4$ in CH_3CN and ∼2 mg of silver nitrate ($AgNO_3$, 99.9999% trace metal basis, Sigma-Aldrich). During electrochemical experiments, the Nernstian potential of the solution was determined by a cyclic voltammetric (CV) measurement of the behavior of a Pt wire electrode (0.5 mm diameter, 99.99% trace metals basis, Sigma-Aldrich) vs the Ag^+/Ag reference electrode.[24]

2. Redox Couples. For redox couples that were not generated by bulk electrolysis and whose concentrations were not limited by solubility considerations,[25] the concentrations of the redox couples were generally 50−65 mM for the species that accepted minority photocarriers and 0.5−5 mM for the species that accepted majority carriers (Table 1). Several of the redox couples contained unstable active species that required in situ generation via bulk electrolysis, as denoted with an asterisk in Table 1. For those systems, the complementary redox species was generated at a large-area Pt gauze electrode (100 mesh, 99.9% trace metals basis, Sigma-Aldrich). Prior to use, all of the Pt electrodes were etched briefly in a 3:1 (v:v) solution of concentrated hydrochloric acid:nitric acid ("aqua regia"), rinsed with water, and thoroughly dried. The Pt gauze working electrode was scanned potentiostatically vs the Ag^+/Ag reference electrode. The counter electrode was a separate piece of Pt gauze that was located in a compartment that was isolated from the main cell by a Vycor frit.

For each redox couple A/A^-, cyclic voltammetric scans of the Pt wire electrode relative a Ag^+/Ag reference electrode, before and after the addition of ferrocene to the solution, were used to establish the Nernstian potential of the cell, $E(A/A^-)$, as well as the formal potential, $E^{o\prime}(A/A^-)$, of the redox system relative to the formal potential of ferrocene$^{+/0}$, $E^{o\prime}$(ferrocene$^{+/0}$) (Table 1). Cyclic voltammetry indicted that ferrocene$^{+/0}$ with 1 M $LiClO_4$ in CH_3CN had a formal potential of $E^{o\prime}$(ferrocene$^{+/0}$) = 0.311 V vs a standard calomel electrode, SCE, in agreement with previous results.[26,27] Table 1 also lists values for the effective solution potential, $E_{eff}(A/A^-)$, that was necessary for the investigation of the dependence of the open-circuit voltage, V_{oc}, on $E(A/A^-)$.[28] The Supporting Information section details the calculation of $E_{eff}(A/A^-)$ based on the value of $E(A/A^-)$ and the concentrations of reduced and oxidized species in each system.

3. Methods. Photoelectrochemical experiments consisted of current−potential sweeps of the Si working electrode versus the Pt wire electrode that was poised at the Nernstian potential, $E(A/A^-)$, of the cell. The $J-E$ data were collected at 50 mV s^{-1} by use of a Gamry Reference 600 potentiostat. Si samples were illuminated with a 300 W ELH-type tungsten-halogen lamp at a light intensity that produced a shortcircuit current density on a calibrated Si photodiode equivalent to that produced by illumination with 100 mW cm^{-2} of Air Mass 1.5 Global sunlight. Open-circuit voltage, V_{oc}, data were directly measured as the photovoltage produced between the semiconductor working electrode and an electrode that was poised at the Nernstian potential of the solution, $E(A/A^-)$, as is appropriate for a two-electrode regenerative photoelectrochemical cell that utilizes one-electron, reversible redox species in the electrolyte.

Area-corrected differential capacitance−potential ($A^2C_{diff}^{-2}-E$, Mott−Schottky)[29,30] data of H-terminated and CH_3-terminated Si(111)/liquid junctions were obtained by the use of electrochemical impedance spectroscopy. Impedance spectra for CH_3-terminated and H-terminated p-Si(111) electrodes in contact with 1,1′-dicarbomethoxycobaltocene$^{+/0}$ in CH_3CN−1.0 M $LiClO_4$ were acquired with the Gamry potentiostat. Impedance data were also recorded for CH_3-terminated and H-terminated electrodes n-Si(111) electrodes in contact with octamethylferrocene$^{+/0}$ in CH_3CN−1.0 M $LiClO_4$. A sinusoidal, 10 mV_{RMS} AC signal that was scanned between 10^{-1} and 10^6 Hz was superimposed on each DC potential. The DC potentials were stepped between 0 and −0.500 V for p-Si electrodes and in a sequence from 0 to 0.400 V for n-Si electrodes. All measurements were performed in stirred solutions in the absence of illumination.

The electrochemical impedance data were fit to a model that consisted of a parallel resistor and capacitor arranged electrically in series with a separate resistor.[4,29,30] Analysis of the impedance data was performed using a custom LabVIEW

program. Data were fit only in the frequency regime in which the parallel capacitance dominated the impedance, generally between 10^3 and 10^5 Hz. The differential capacitance, C_{diff}, approximated the capacitance of the semiconductor space-charge region, C_{sc}, yielding the flat-band potential, E_{fb}, through the Mott–Schottky relationship, eq 1.

$$A^2 C_{diff}^{-2} = \frac{2}{q\epsilon\epsilon_0 N_D}\left(E - E_{fb} - \frac{k_B T}{q}\right) \quad (1)$$

In eq 1, A is the area of the semiconductor-liquid junction, ϵ is the dielectric constant of Si, ϵ_0 is the permittivity of vacuum, N_D is the doping density of the sample, T is the absolute temperature, k_B is Boltzmann's constant, and q is the (unsigned) charge on an electron.

III. RESULTS

A. Current–Potential Behavior of H-Terminated vs CH_3-Terminated Si Electrodes in Contact with Various Redox Couples in CH_3CN. Figure 1 presents representative

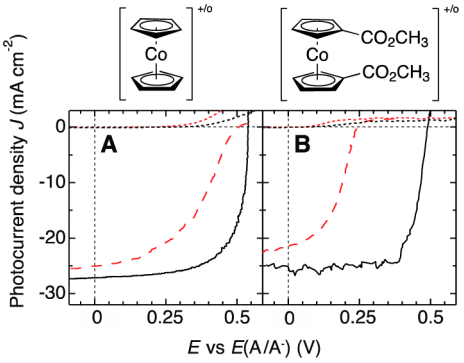

Figure 1. Photocurrent density-potential (J–E) performance of p-Si electrodes in contact with cobaltocene$^{+/0}$ (frame A) and in contact with 1,1′-dicarbomethoxycobaltocene$^{+/0}$ (frame B) in CH_3CN–1.0 M $LiClO_4$. In contact with cobaltocene$^{+/0}$ (frame A), both a H-terminated (black, solid trace) and a CH_3-terminated (red, dashed trace) p-Si electrode exhibited high V_{oc} values. Conversely, contact with 1,1′-dicarbomethoxycobaltocene$^{+/0}$ resulted in decreased V_{oc} values for CH_3-terminated p-Si(111) compared to the V_{oc} for H-terminated p-Si(111) surfaces. In both frames, the black and red dotted traces represent the J–E response in the absence of illumination for the H-terminated and CH_3-terminated p-Si(111) electrodes, respectively.

J–E data for selected p-Si(111) semiconductor-liquid junctions under 100 mW cm^{-2} of ELH-type illumination. In contact with CH_3CN-$CoCp_2^{+/0}$, p-type H–Si(111) and p-type CH_3–Si(111) electrodes exhibited rectifying behavior, showing cathodic photocurrent, and showing significant anodic current in the dark only at positive potentials vs $E(A/A^-)$. Under the specified illumination conditions, the p-type H–Si(111) electrode exhibited an open-circuit voltage V_{oc}, of 538 mV, whereas V_{oc} = 504 mV for the p-type CH_3–Si(111) electrode (Figure 1A). In contrast, in contact with CH_3CN-1,1′-dicarbomethoxycobaltocene$^{+/0}$, the p-type H–Si(111) electrodes exhibited V_{oc} = 489 mV while the p-type CH_3–Si(111) electrode yielded V_{oc} = 202 mV (Figure 1B).

Figure 2 presents representative J–E data for n-type Si electrodes. In contact with CH_3CN–acetylferrocene$^{+/0}$, n-type H–Si(111) and n-type CH_3–Si(111) electrodes exhibited rectifying behavior, showing anodic photocurrent and showing

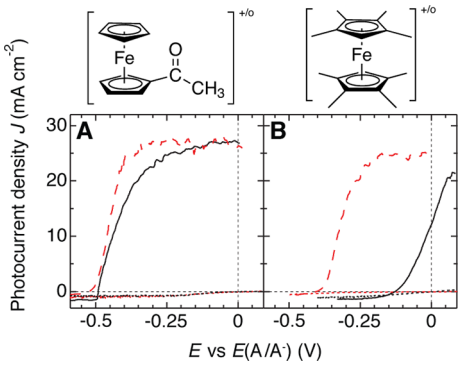

Figure 2. J–E behavior for n-Si electrodes in contact with acetylferrocene$^{+/0}$ (frame A) and in contact with octamethylferrocene$^{+/0}$ (frame B) in CH_3CN–1.0 M $LiClO_4$. In contact with acetylferrocene $^{+/0}$ in frame A, both a H-terminated (black, solid trace) and a CH_3-terminated (red, dashed trace) n-Si electrode exhibited high V_{oc} values. Conversely, contact with octamethylferrocene$^{+/0}$ resulted in a larger V_{oc} value for CH_3-terminated n-Si(111) compared to the V_{oc} for the H-terminated n-Si(111) surfaces. In both frames, the black and red dotted traces represent the J–E response in the absence of illumination for the H-terminated and CH_3-terminated p-Si(111) electrodes, respectively.

significant cathodic current in the dark only at negative potentials vs $E(A/A^-)$. For the system in Figure 2, the n-type H–Si(111) electrode exhibited V_{oc} = −495 mV, whereas the n-type CH_3–Si(111) electrode exhibited V_{oc} = −525 mV (frame A). In contrast, in contact with CH_3CN–octamethylferrocene$^{+/0}$, the n-type CH_3–Si(111) electrode exhibited a V_{oc} = −406 mV but the n-type H–Si(111) electrode showed V_{oc} = −129 mV (frame B).

Figure 3 presents the dependence of V_{oc} on the effective solution potential, $E_{eff}(A/A^-)$, for p-type CH_3–Si(111) (black, open squares), p-type H–Si(111) (green, filled squares), n-type CH_3–Si(111) (red, open circles), and n-type H–Si(111) (blue, filled circles) in contact with 1.0 M $LiClO_4$–CH_3CN under 100 mW cm^{-2} of ELH-simulated AM 1.5 illumination. Each point represents an average of at least 5 electrodes with values and standard deviations listed in Table 1. To highlight the observed trends for each series of electrodes, the empirically determined guide lines included in Figure 3 separately denote the region of low V_{oc}; a region over which V_{oc} scaled approximately linearly with $E_{eff}(A/A^-)$, with a slope of 1; and a region of maximized V_{oc}, in which V_{oc} was independent $E_{eff}(A/A^-)$.[31]

B. Differential Capacitance–Potential Behavior. Figure 4 plots the electrode area-corrected differential capacitance vs potential ($A^2C_{diff}^{-2}$–E) response for n-type H–Si(111) and n-type CH_3–Si(111) electrodes in contact with octamethylferrocene$^{+/0}$–1.0 M $LiClO_4$–CH_3CN (frame A) as well as for p-type H–Si(111) and p-type CH_3–Si(111) electrodes in contact with 1,1′-dicarbomethoxycobaltocene$^{+/0}$–1.0 M $LiClO_4$–CH_3CN (frame B). The flat-band potential, E_{fb}, was determined using the x-intercept extrapolation in Figure 4, in conjunction with eq 1. For the n-type Si electrodes (frame A), E_{fb} shifted from −271 mV vs E(octamethylferrocene$^{+/0}$) for the H–Si(111) electrode to −660 mV vs E(octamethylferrocene$^{+/0}$) for the CH_3–Si(111) electrode. The average shift in E_{fb} for three electrodes of n-type H–Si(111) relative to the E_{fb} value for three electrodes of n-type CH_3–Si(111) electrodes in octamethylferrocene$^{+/0}$–1.0 M $LiClO_4$–CH_3CN was −0.40 V. For the p-Si electrodes in Figure 4B, E_{fb} shifted from 679 mV vs E(1,1′-dicarbomethoxycobaltocene$^{+/0}$) for the H–Si(111) electrode to

dx.doi.org/10.1021/jp308461q | J. Phys. Chem. C 2012, 116, 23569–23576

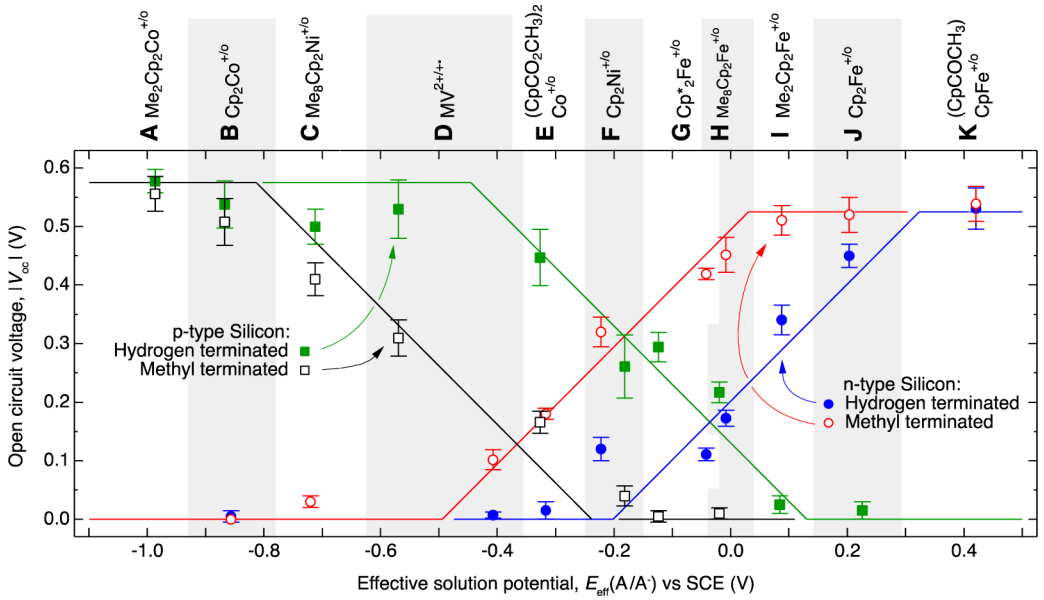

Figure 3. Open-circuit voltage, V_{oc}, vs effective solution redox potential, $E_{eff}(A/A^-)$, in CH_3CN−1.0 M $LiClO_4$ for H-terminated p-Si(111) (green, solid squares), CH_3-terminated p-Si(111) (black, hollow squares), H-terminated n-Si (blue, solid squares), and CH_3-terminated n-Si(111) (red, hollow squares) electrodes. The corresponding lines serve as guides to indicate the observed trends in the different regions of V_{oc} vs $E_{eff}(A/A^-)$ behavior.

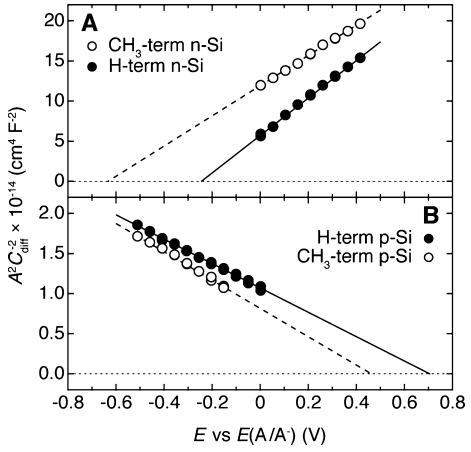

Figure 4. Differential capacitance−potential, $A^2C_{diff}^{-2}$−E, relationships for n-Si(111) electrodes in octamethylferrocene$^{+/0}$ (frame A) and p-Si(111) electrodes in 1,1′-dicarbomethoxycobaltocene$^{+/0}$ (frame B) for H-terminated electrodes (solid circles, solid linear extrapolation to $A^2C_{diff}^{-2}$ = 0 cm^4 F^{-2}) and CH_3-terminated electrodes (open circles, dashed linear extrapolation to $A^2C_{diff}^{-2}$ = 0 cm^4 F^{-2}). The change in potential values in the extrapolation to $A^2C_{diff}^{-2}$ = 0 cm^4 F^{-2} corresponds to a negative shift in the flat-band potential for CH_3-terminated Si(111) electrodes relative to the flat band potential of H-terminated Si(111) electrodes in contact with these selected redox systems.

437 mV vs E(1,1′-dicarbomethoxycobaltocene$^{+/0}$) for the CH_3−Si(111) electrode. The average shift in E_{fb} for three electrodes of p-type H−Si(111) relative to the E_{fb} for three electrodes of p-type CH_3−Si(111) in 1,1′-dicarbomethoxycobaltocene$^{+/0}$−1.0 M $LiClO_4$−CH_3CN was 0.25 V.

IV. DISCUSSION

Upon functionalization of the surface, a change in the open-circuit photovoltage of a photoelectrode in contact with an single redox system could indicate a shift in the interfacial dipole, a change in the surface recombination rate, and/or a change in the position of the surface Fermi level due to Fermi level pinning. However, the systematic shift in V_{oc} observed herein for a series of electrochemically reversible, one-electron transfer, outer-sphere, redox couples (Figure 3) strongly indicates that a change in the magnitude of the interfacial dipole is the predominant electrical effect that accompanies a change in the chemical termination of the Si(111) surface from H− to CH_3− moieties. This hypothesis is consistent with the observation that the photovoltage exhibits nearly identical maximal limiting values at very positive values of $E(A/A^-)$ for the n-type electrodes of both functionality, and exhibits similar maximal limiting values at very negative values of $E(A/A^-)$ for the p-type Si electrodes.[31] Furthermore, the potential shift of the band-edges observed in selected cases by the $A^2C_{diff}^{-2}$−E measurements (Figure 4) unambiguously indicates that the interfacial dipole has been modified by the surface functionalization procedure. The observation of the dependence of V_{oc} on $E(A/A^-)$ for a wide range of Nernst potentials of the solution indicates that the functionalization has not also introduced deleterious increases in the rates of surface recombination processes nor has deleteriously affected the rates of interfacial minority-carrier transfer to the redox species in the electrolyte. The CH_3− functionalization thus for all practical purposes yields the same, nearly ideal, electrical behavior that is characteristic of H−Si(111) surfaces but with a shift in the interfacial dipole, and thus in the band-edge positions, for CH_3−Si(111) surfaces, along with improved resistance to chemical and electrochemical oxidation processes that accompanies the replacement of Si−H bonds by surficial Si−C bonds. For a given value of $E(A/A^-)$, the shift in interfacial dipole produces larger photovoltages for n-type Si photoelectrodes and smaller photovoltages for p-type Si photocathodes, until the limiting regimes of maximal V_{oc} (or minimal V_{oc}) are reached at very negative or at very positive potentials, respectively (Figure 3).

dx.doi.org/10.1021/jp308461q | J. Phys. Chem. C 2012, 116, 23569−23576

From the impedance experiments, the shift in E_{fb} due to surface methylation was −0.40 V for n-Si(111) electrodes in contact with octamethylferocene$^{+/0}$−CH_3CN and −0.25 V for p-Si(111) electrodes in contact with 1,1′-dicarbomethoxycobaltocene$^{+/0}$−CH_3CN, relative to the E_{fb} behavior of the respective H−Si(111) electrode surfaces. The magnitude of this E_{fb} shift is broadly consistent with the −0.3 V shift in the guide lines in Figure 3 between the V_{oc} trends for CH_3−Si(111) and H−Si(111) electrodes. The flat-band shifts observed for the Si/CH_3CN junctions are somewhat smaller than the ∼−0.49 eV dipole energy shift that has been reported between CH_3−Si(111) and H−Si(111) surfaces in ultrahigh vacuum as measured by photoelectron spectroscopy.[9,15−17] Shifts of ∼−0.55 eV in the band-edge positions have been inferred from measurements of changes in the barrier heights of silicon/mercury contacts.[4] The reduction in the magnitude of the interfacial dipole at semiconductor/liquid contacts relative to ultrahigh vacuum experiments is consistent with a partial screening of the dipole by the electrolyte and/or inherent shifts in the band-edge positions of Si in contact with an electrolyte relative to the band-edge positions in contact with UHV.

The sign and approximate magnitude of the interfacial dipole that results from H− or CH_3− termination has been evaluated theoretically.[18] Broadly, the sign of the interfacial dipole is in accord with the electronegativity differences between Si and either H− or CH_3− moieties. Using both density functional theory and many-body perturbation theory, specifically the perturbative G_oW_o approach, a band-edge shift of −0.8 eV has been predicted for CH_3−Si(111) surfaces relative to H−Si(111) surfaces in contact with vacuum and thus in the absence of solvation or specific adsorption.[18] The sign and magnitude of the interfacial dipole layer indicated by the data described herein is therefore consistent with theoretical expectations for this type of surface functionalization process.

The band−edge shift that accompanies CH_3-termination of Si(111) is advantageous for some applications and disadvantageous for others. For example, with a given redox system, the shift that results from CH_3-termination of Si(111) is expected to produce higher barrier heights and thus higher photovoltages and better rectification, for n-Si(111) photoanodes, but also is expected to result in poorer ohmic contacts between a low work function conducting polymer, such as poly(3,4-ethylenedioxythiophene)/poly(styrenesulfonate) (PEDOT/PSS) and n-type CH_3-terminated Si(111) surfaces.[32] Similarly, the band-edge shift introduced by CH_3-termination will produce better ohmic contacts, but smaller photovoltages, for photocathodes that are formed from CH_3-functionalized p-Si(111) electrodes relative to photocathodes formed from H-terminated p-Si(111) electrodes.[33] The improved oxidation resistance upon functionalization of Si(111) with methyl groups[34] thus is accompanied by a decrease in the photoelectrochemical performance of Si(111) surfaces for photocathodic proton reduction in solar-driven water-splitting systems.[3] These expectations are in accord with experimental observations on H−Si(111) vs CH_3−Si(111) electrodes to date.[14,33,34] Hence, alternate routes to surface functionalization that shift the band-edge positions positively and/or the use of buried p−n^+ junctions[35,36] will be required to combine the improved stability with improvements in open-circuit photovoltages upon functionalization of p-Si(111) photocathodes.

V. CONCLUSIONS

For a given solution redox potential, CH_3-terminated p-Si(111) electrodes showed lower V_{oc} values than H-terminated p-Si(111) electrodes, whereas CH_3-terminated n-type Si(111) electrodes showed higher V_{oc} values than H-terminated n-Si(111) electrodes. Differential capacitance−potential experiments confirmed that differences between the flat-band potentials of CH_3−Si(111) electrodes and H−Si(111) yielded the respective V_{oc} vs $E(A/A^-)$ behavior. The observed changes in flat-band potential are consistent with a negative shift in the interfacial dipole as a result of methylation of the Si(111) surface and indicate that, relative to the behavior of H−Si(111) electrodes, methylation of Si(111) increases the rectifying behavior at n-type Si/liquid junctions and increases the ohmic behavior of p-type Si/liquid junctions. The shift in flat-band potential observed electrochemically is fully consistent with the shift in interfacial dipole observed by photoemission in ultrahigh vacuum, as well as by the electrical behavior of Si/Hg contacts and additionally as predicted theoretically by density functional theory.

■ ASSOCIATED CONTENT

Supporting Information

Calculation of effective solution potential, $E_{eff}(A/A^-)$, and X-ray photoelectron spectra quantifying the degree of oxidation on the methylated Si(111) surfaces. This material is available free of charge via the Internet at http://pubs.acs.org.

■ AUTHOR INFORMATION

Corresponding Author

*E-mail: nslewis@caltech.edu.

Notes

The authors declare no competing financial interest.

■ ACKNOWLEDGMENTS

We acknowledge the National Science Foundation (CHE-1214152 and CHE-0911682) and the Molecular Materials Research Center of the Beckman Institute at the California Institute of Technology for supporting this work. The authors thank Dr. David Knapp for his synthesis of 1,1′-dicarbomethoxycobaltocene$^{+/0}$ as well as Dr. Chengxiang Xiang and Professor Erik Johansson for helpful discussions.

■ REFERENCES

(1) Tan, M. X.; Laibinis, P. E.; Nguyen, S. T.; Kesselman, J. M.; Stanton, C. E.; Lewis, N. S. *Prog. Inorg. Chem.* **1994**, *41*, 21.

(2) Bard, A. J.; Faulkner, L. R. *Electrochemical Methods: Fundamentals and Applications*, 2nd ed.; Wiley: New York, 2001.

(3) Walter, M. G.; Warren, E. L.; McKone, J. R.; Boettcher, S. W.; Mi, Q. X.; Santori, E. A.; Lewis, N. S. *Chem. Rev.* **2010**, *110*, 6446.

(4) Maldonado, S.; Plass, K. E.; Knapp, D.; Lewis, N. S. *J. Phys. Chem. C* **2007**, *111*, 17690.

(5) Webb, L. J.; Nemanick, E. J.; Biteen, J. S.; Knapp, D. W.; Michalak, D. J.; Traub, M. C.; Chan, A. S. Y.; Brunschwig, B. S.; Lewis, N. S. *J. Phys. Chem. B* **2005**, *109*, 3930.

(6) Webb, L. J.; Rivillon, S.; Michalak, D. J.; Chabal, Y. J.; Lewis, N. S. *J. Phys. Chem. B* **2006**, *110*, 7349.

(7) Bansal, A.; Li, X. L.; Lauermann, I.; Lewis, N. S.; Yi, S. I.; Weinberg, W. H. *J. Am. Chem. Soc.* **1996**, *118*, 7225.

(8) Bansal, A.; Li, X. L.; Yi, S. I.; Weinberg, W. H.; Lewis, N. S. *J. Phys. Chem. B* **2001**, *105*, 10266.

(9) Hunger, R.; Fritsche, R.; Jaeckel, B.; Jaegermann, W.; Webb, L. J.; Lewis, N. S. *Phys. Rev. B* **2005**, *72*.

(10) Yu, H. B.; Webb, L. J.; Ries, R. S.; Solares, S. D.; Goddard, W. A.; Heath, J. R.; Lewis, N. S. *J. Phys. Chem. B* **2005**, *109*, 671.
(11) Royea, W. J.; Juang, A.; Lewis, N. S. *Appl. Phys. Lett.* **2000**, *77*, 1988.
(12) Hunger, R.; Fritsche, R.; Jaeckel, B.; Webb, L. J.; Jaegermann, W.; Lewis, N. S. *Surf. Sci.* **2007**, *601*, 2896.
(13) Jaeckel, B.; Hunger, R.; Webb, L. J.; Jaegermann, W.; Lewis, N. S. *J. Phys. Chem. C* **2007**, *111*, 18204.
(14) Bansal, A.; Lewis, N. S. *J. Phys. Chem. B* **1998**, *102*, 1067.
(15) Akremi, A.; Lacharme, J. P.; Sebenne, C. A. *Surf. Sci.* **1998**, *404*, 746.
(16) Hunger, R.; Pettenkofer, C.; Scheer, R. *J. Appl. Phys.* **2002**, *91*, 6560.
(17) Hollinger, G.; Himpsel, F. J. *J. Vac. Sci. Technol. A* **1983**, *1*, 640.
(18) Li, Y.; O'Leary, L. E.; Lewis, N. S.; Galli, G. *Energy Environ. Sci.*, submitted.
(19) Kern, W. Overview and Evolution of Silicon Wafer Cleaning Technology. In *Handbook of Silicon Wafer Cleaning Technology*, 2nd ed.; Reinhardt, K. A., Kern, W., Eds.; William Andrew Publishing, 2008.
(20) Inyushin, S.; Shafir, A.; Sheats, J. E.; Minihane, M.; Whitten, C. E.; Arnold, J. *Polyhedron* **2004**, *23*, 2937.
(21) Hart, W. P.; Macomber, D. W.; Rausch, M. D. *J. Am. Chem. Soc.* **1980**, *102*, 1196.
(22) Sheats, J. E.; Rausch, M. D. *J. Org. Chem.* **1970**, *35*, 3245.
(23) Hendrickson, D. N.; Sohn, Y. S.; Gray, H. B. *Inorg. Chem.* **1971**, *10*, 1559.
(24) Smith, T. J.; Stevenson, K. J. Reference Electrodes. In *Handbook of Electrochemistry*; Zoski, C. G., Ed.; Elsevier: Amsterdam, 2007.
(25) Robbins, J. L.; Edelstein, N.; Spencer, B.; Smart, J. C. *J. Am. Chem. Soc.* **1982**, *104*, 1882.
(26) Connelly, N. G.; Geiger, W. E. *Chem. Rev.* **1996**, *96*, 877.
(27) Kuwana, T.; Bublitz, D. E.; Hoh, G. *J. Am. Chem. Soc.* **1960**, *82*, 5811.
(28) Rosenbluth, M. L.; Lewis, N. S. *J. Phys. Chem.* **1989**, *93*, 3735.
(29) Fajardo, A. M.; Lewis, N. S. *J. Phys. Chem. B* **1997**, *101*, 11136.
(30) Gstrein, F.; Michalak, D. J.; Knapp, D. W.; Lewis, N. S. *J. Phys. Chem. C* **2007**, *111*, 8120.
(31) Lewis, N. S. *J. Electrochem. Soc.* **1984**, *131*, 2496.
(32) Yahyaie, I.; McEleney, K.; Walter, M. G.; Oliver, D. R.; Thomson, D. J.; Freund, M. S.; Lewis, N. S. *J. Phys. Chem. C* **2011**, *115*, 24945.
(33) Johansson, E.; Boettcher, S. W.; O'Leary, L. E.; Poletayev, A. D.; Maldonado, S.; Brunschwig, B. S.; Lewis, N. S. *J. Phys. Chem. C* **2011**, *115*, 8594.
(34) Hamann, T. W.; Lewis, N. S. *J. Phys. Chem. B* **2006**, *110*, 22291.
(35) Warren, E. L.; Boettcher, S. W.; Walter, M. G.; Atwater, H. A.; Lewis, N. S. *J. Phys. Chem. C* **2011**, *115*, 594.
(36) Boettcher, S. W.; Warren, E. L.; Putnam, M. C.; Santori, E. A.; Turner-Evans, D.; Kelzenberg, M. D.; Walter, M. G.; McKone, J. R.; Brunschwig, B. S.; Atwater, H. A.; Lewis, N. S. *J. Am. Chem. Soc.* **2011**, *133*, 1216.